Electronic Supplementary Information

High-efficiency oxygen evolution catalyzed by Sn-Co-Ni phosphide with oriented crystal phases

Xin Liu,[a] Jun Huang,[b,c] Tongtong Li,*[a] Wei Chen,*[b] Guangliang Chen,*[a] Liting Han[b] and Kostya (Ken) Ostrikov[c]

[a]School of Materials Science and Engineering, Zhejiang Sci-Tech University, Hangzhou 310018, P. R. China

*E-mail: glchen@zstu.edu.cn; yitaji@zstu.edu.cn

[b]School of Physics and Electronic Information, Gannan Normal University, Ganzhou, Jiangxi 341000, P. R. China

*E-mail: chwbetter@163.com

[c]School of Chemistry and Physics, Centre for Materials Science, Centre for Clean Energy Technologies and Practices, Centre for Waste-free World, Queensland University of Technology (QUT), Brisbane, QLD 4000, Australia

1. Experimental

1.1 Chemicals and Reagents

Ni-Co foam (NCF, thickness: 1 mm) with different Ni/Co ratios (1:8, 1:7, 1:6) was purchased from Suzhoutaili Co., Ltd. Ethyl alcohol (CH_3CH_2OH, ≥ 99.7 %), acetone (CH_3COCH_3, ≥ 99.5 %), stannous chloride dihydtrate ($SnCl_2{\cdot}2H_2O$), sulfuric acid (H_2SO_4, ≥ 99.5 %), red phosphorus (P_4, 98.5 %), potassium hydroxide (KOH, ≥ 85.0 %), carbon electrode (6 mm), and ruthenium oxide (RuO_2, 99.9 %) were purchased from the Hangzhou Minling Chemical Instrument Co., Ltd. Deionized water was used in all experiments, and all the chemical reagents were of analytical grade.

1.2 *In-situ* fabrication of Sn/NCF

Before the electro-deposition, the NCF (1 × 1 cm) was cleaned with acetone and 10 % wt hydrochloric acid solution for 15 min in an ultrasound bath, and followed by three times of cleaning with ethanol and deionized water. Then, the Sn nano-particles were grown on the NCF at -0.6 V in three-electrode system for 100 s. The NCF was used as working electrode, while carbon electrode and Hg/Hg_2Cl_2 were served as counter and reference electrode, respectively. The whole electrode setup was dipped into 30 mL of electrolyte solution composed of 0.03 M $SnCl_2{\cdot}H_2O$ and 0.5 M H_2SO_4. The resulting sample was washed with deionized water for three times. Lastly, the Sn/NCF sample was dried in an oven with a temperature of 40 °C for 1 h. For comparison, the samples with different Ni/Co ratio, electro-deposition potential, electro-deposition time and electrolyte concentration were also fabricated with similar conditions.

1.3 Synthesis of SnPi@CoP-Ni_5P_4/NCF samples

The as-prepared Sn/NCF and 0.3 g red phosphorus powders were respectively placed at downstream and upstream of the porcelain boat in a chemical vapor deposition (CVD) system. Subsequently, the samples were heated to 550 °C with a heating rate of 5 °C/min and maintained for 2.5 h in the P + N_2 (Pressure: 50 Pa). After the phosphorization process, the sample was cooled down to the environment temperature under N_2 (25 sccm) flow, and labelled as SnPi@CoP-Ni_5P_4/NCF sample. For comparison, the sample was also obtained with the different reactive conditions in the CVD system, such as different reaction temperature, reaction time, and amount of red phosphorus.

1.4 Synthesis of $NiCoP_x$/NCF samples

The as-cleaned NCF and 0.3 g red phosphorus powders were placed at downstream and upstream of the porcelain boat in a chemical vapor deposition (CVD) system, respectively. Subsequently, the samples were heated to 550 °C with a heating rate of 5 °C/min and maintained for 2.5 h in the P + N_2 (Pressure: 50 Pa). After phosphorization process, the sample was cooled down to the environmental temperature under N_2 (25 sccm) flow, and labelled as $NiCoP_x$/NCF sample.

1.5 Synthesis of Ni_2O_3-$CoSnO_3$/NCF samples

The Sn/NCF precursor was placed at the porcelain boat in a chemical vapor deposition (CVD) system. Subsequently, the samples were heated to 550 °C with a heating rate of 5 °C/min and maintained for 2.5 h in the N_2 (Pressure: 50 Pa). After high-temperature reaction process, the sample was cooled down to the environment temperature under N_2 (25 sccm) flow, and labelled as Ni_2O_3-$CoSnO_3$/NCF sample.

1.6 Materials characterization

The physico-chemical structures of the catalysts are investigated with following instruments. The surface morphology was characterized by using the field-emission scanning electron microscopy (FE-SEM, JSM-6700F, Japan) and transmission electron microscopy (TEM, Model JSM-2100, JEOL, Japan). The energy dispersive spectroscopy (EDS) elemental maps were produced by the aberration-corrected high angle annular dark field scanning transmission electron-microscopy (HAADF-STEM, FEI Titan G2, USA) with an operating voltage of 300 kV. The crystal phases and chemical state were determined by the X-ray diffractometer (XRD, Thermo Fisher Scientific, USA) equipped a Cu Kα radiation source (35 kV) and the X-ray photoelectron spectroscopy (XPS, K-Alpha, USA) with the X-ray source (Al Kα: 1486.6 eV). The frame structures of catalysts before and after a long-time electrocatalytic processes were checked by a Raman spectroscope (Model: Lab Ram HRUV).

1.7 Electrochemical measurements

The electrocatalytic performances of the produced samples were measured with a conventional electrochemical workstation (Model CHI 660E, Shanghai Chenhua Instrument Co., Ltd.), whereas the sample, Hg/Hg_2Cl_2 (saturated KCl solution) and carbon rod (6 mm) acted as working, reference and counter electrodes in alkaline electrolyte (1 M KOH, pH 14), respectively. The measured potential is converted to RHE according to the following equation:

E vs RHE = E vs Hg/Hg_2Cl_2 + 0.241 + 0.059 pH.

The resulting polarization curves were *iR*-compensated according to the equation:

$$E_c = E_m - iR_s ,$$

where E_c is the corrected potential, E_m is the measured potential experimentally, R_s is the resistance of the solution obtained from the curve. The working electrode was activated with the cyclic voltammetry (CV) scanning process at a scanning rate of 5 mV s^{-1}. The linear sweep voltammetry (LSV) curves were

measured with a scanning rate of 1 mV s^{-1}. The electrochemical impedance spectrum (EIS) was recorded in the frequency range of 100 kHz ~ 0.01 Hz with a 5 mV AC voltage amplitude at different potentials. The electrocatalytic sustainability of the electrode quantified by the chronoamperometry test was analyzed with potentials of 0.053 V vs RHE (10 mA cm^{-2}) and 0.085 V vs RHE (100 mA cm^{-2}). The stability was determined by the CV measurement at a scan rate of 5 mV s^{-1} and the long-term durability tests, respectively. For comparison, the NCF coated with RuO_2 with a same mass loading rate as the SnPi@CoP-Ni_5P_4/NCF (6.3 mg cm^{-2}) acted as OER electrode, respectively. The electrochemical capacitance at non-Faraday potential (from -0.8 to -0.6 V vs Hg/Hg_2Cl_2) was measured by CV with different scanning speeds (e.g. 20, 60, 100, 140 and 180 mV s^{-1}) to estimate the effective electrochemical surface area (ECSA) by calculating the double layer capacitance (C_{dl}). Finally, the two-electrode electrolytic cell assembled with SnPi@CoP-Ni_5P_4/NCF was investigated to detect the electrocatalytic performances for overall water-splitting. The turnover frequency (TOF) for OER followed the equation: TOF = $I/(4Fn)$, where the I, F, and n denote the current (A), the Faraday constant (C mol^{-1}), and the number of active sites (mol), respectively. The factors of 1/4 or 1/2 are the corresponding electron transfer numbers. In addition, the mechanisms of OER enhancement is explored by *in-situ* Raman system on the inVia Reflex-Renishaw spectrometer (excitation wavelength 532 nm), and the sample was filled in a H-tape in situ cell provided by Beijing Scistar Technology Minling Co., Ltd.

1.8 Quantum chemistry simulation details

The simulations were calculated by spin-polarized first-principles DFT,[S1] which is provided by the Vienna an initio Simulation Package (VASP)[S2] with projector augmented wave (PAW).[S3] The generalized gradient approximation,[S4] developed by Perdew, Burke and Ernzerhof (GGA-PBE), was

used as the exchange correlation functional. The cut-off energy was set to 400 eV. Brillouin zones were sampled by a set of k points grid (3×3×1) according to the Monkhorst-Pack scheme, which has the convergence tolerance of energy changes of 10^{-5} eV. The vdW interaction was introduced to treat the interaction between the molecules and the substrate, and it is described by a semiempirical correction by the DFT - D3 method.[S5] In addition, to evaluate the OER activity of the materials, we calculate the Gibbs free energy of coordinate elementary steps and overpotential for OER based on the following 4e mechanism proposed by Nørskov for water oxidation.[S6]

$$H_2O(l) + * \leftrightharpoons HO^* + H^+ + e^-$$

$$HO^* \leftrightharpoons O^* + H^+ + e^-$$

$$O^* + H_2O(l) \leftrightharpoons HOO^* + H^+ + e^-$$

$$HOO^* \leftrightharpoons * + O_2(g) + H^+ + e^-$$

Here, the symbols "*" denotes the active sites on the catalyst, (*l*) and (*g*) represents liquid and gas phases, respectively. In order to fully discuss the active facet of the catalyst, the (002) and (201) of CoP, the (203) of Ni_5P_4 as well as the (222) of SnP_2O_7 were considered.

2. Supplementary figures

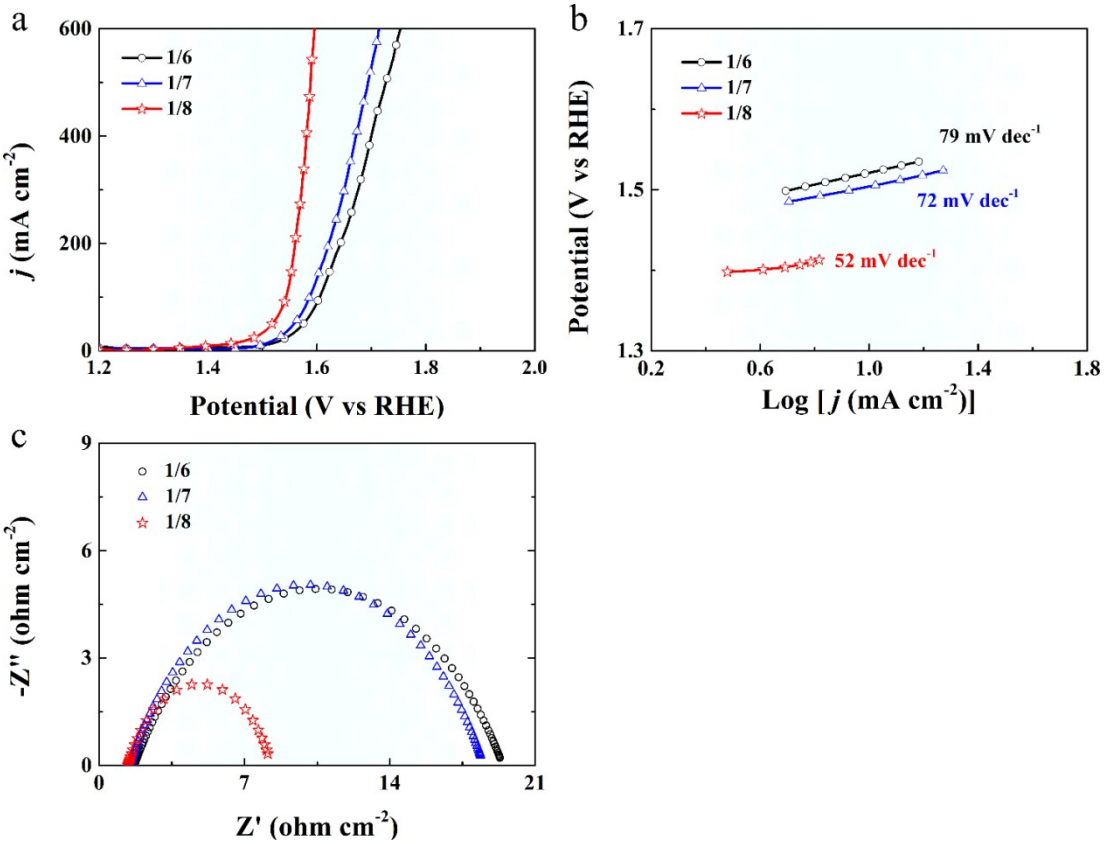

Figure S1. The effect of the different Ni/Co ratio substrate on the OER activity of SnPi@CoP-Ni_5P_4/NCF in 1.0 M KOH electrolyte. (a) LSV curves and the corresponding Tafel slopes (b), and Nyquist curves (c).

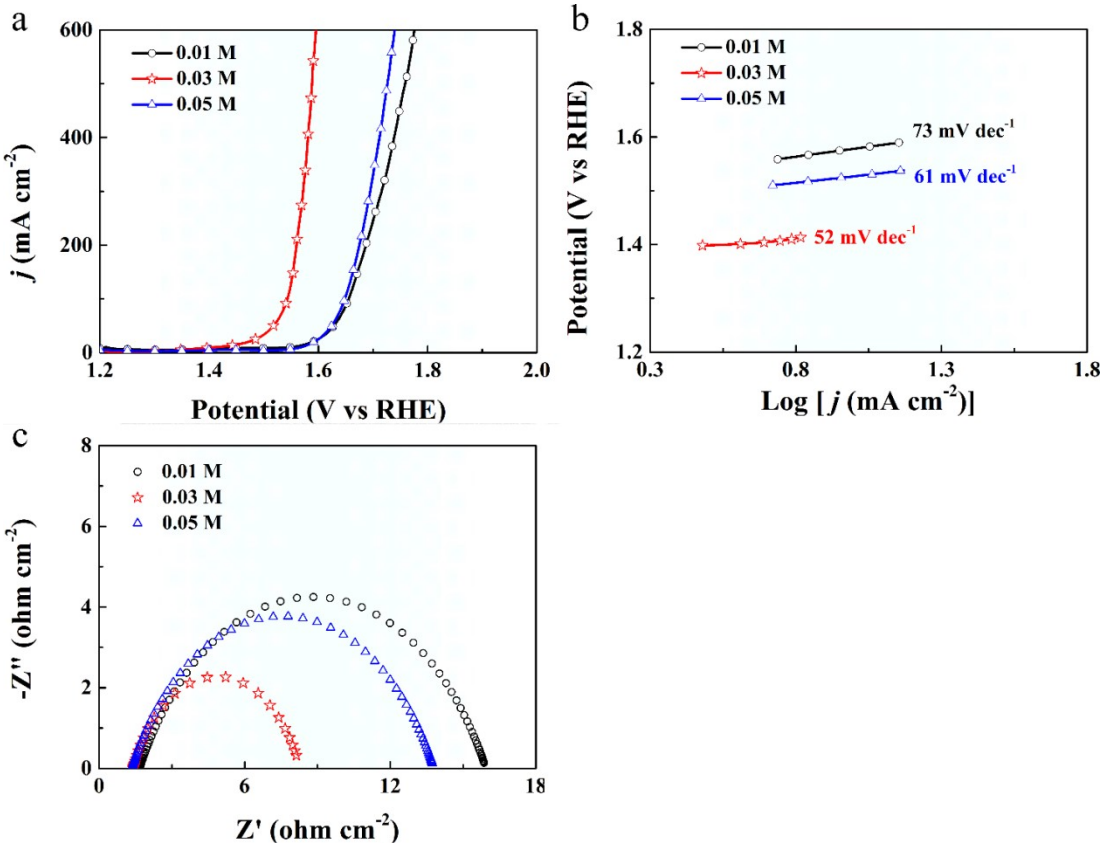

Figure S2. The effect of the electrodeposition solution concentration on the OER activity of SnPi@CoP-Ni_5P_4/NCF in 1.0 M KOH electrolyte. (a) LSV curves and the corresponding Tafel slopes (b), and Nyquist curves (c).

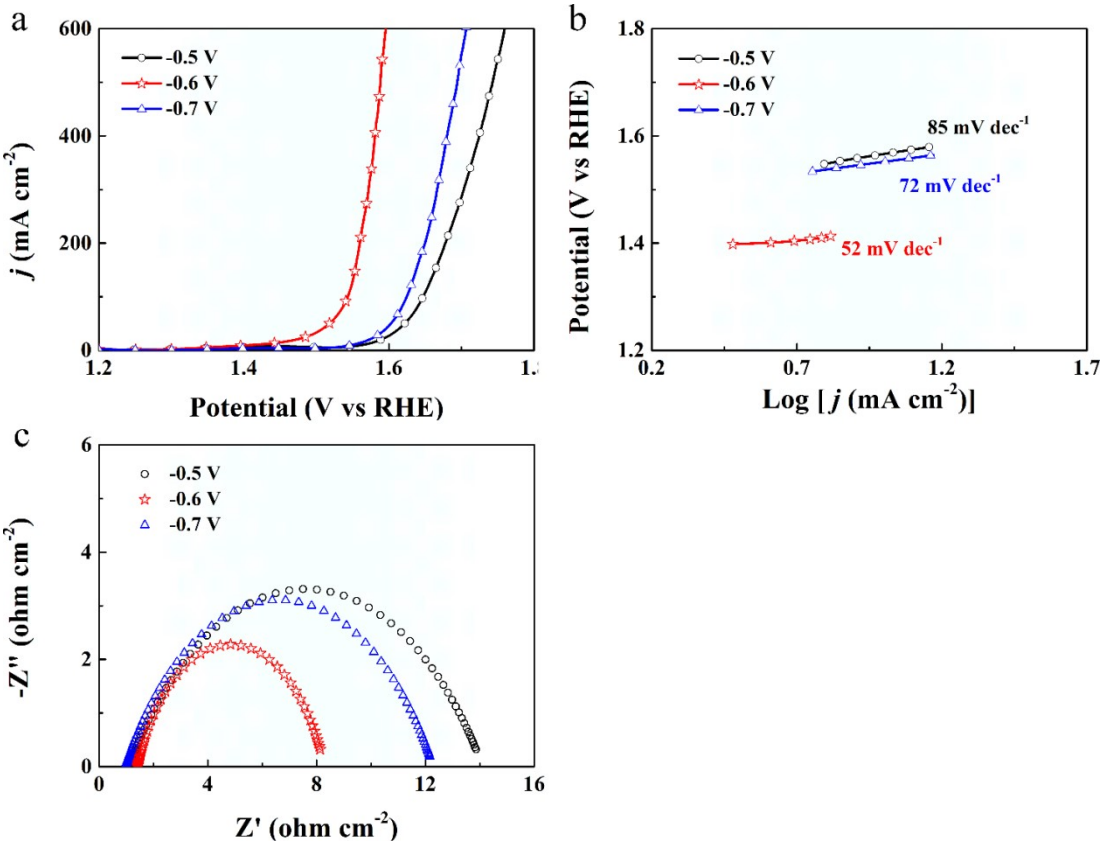

Figure S3. The effect of the electrodeposition potential on the OER activity of SnPi@CoP-Ni_5P_4/NCF in 1.0 M KOH electrolyte. (a) LSV curves and the corresponding Tafel slopes (b), and Nyquist curves (c).

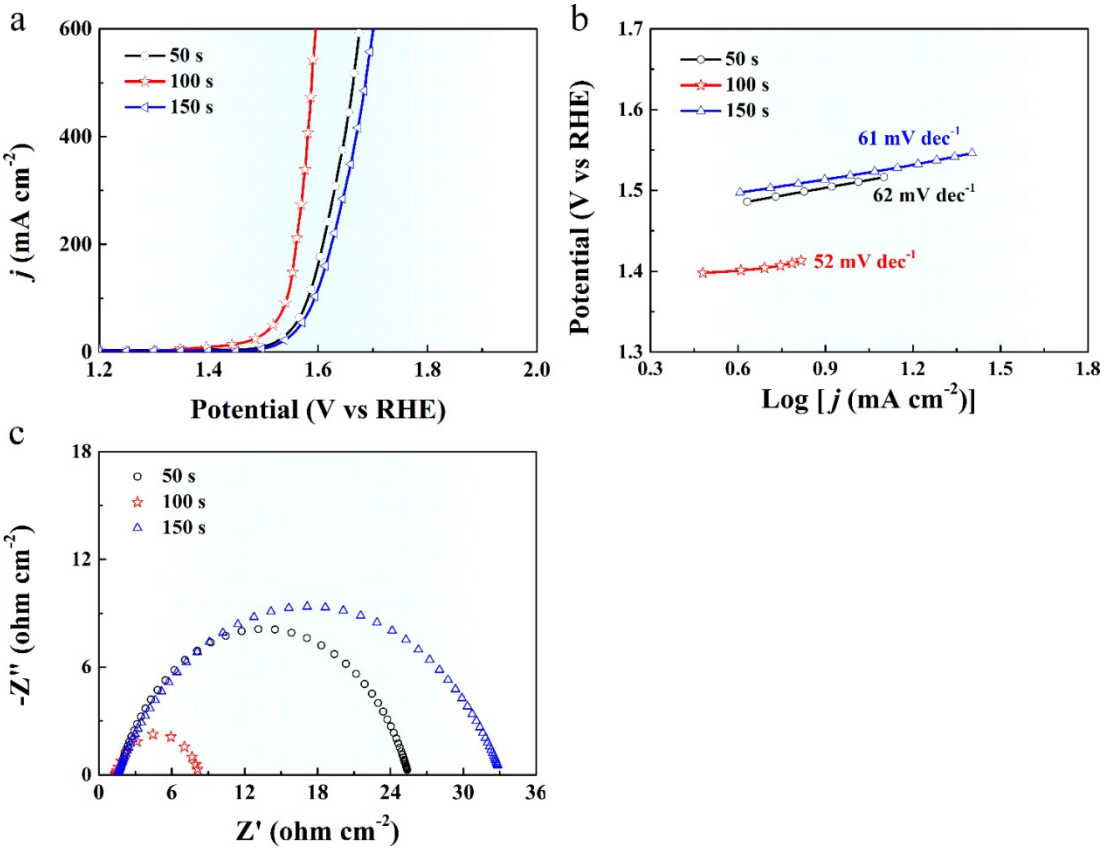

Figure S4. The effect of the electrodeposition time on the OER activity of SnPi@CoP-Ni_5P_4/NCF in 1.0 M KOH electrolyte. (a) LSV curves and the corresponding Tafel slopes (b), and Nyquist curves (c).

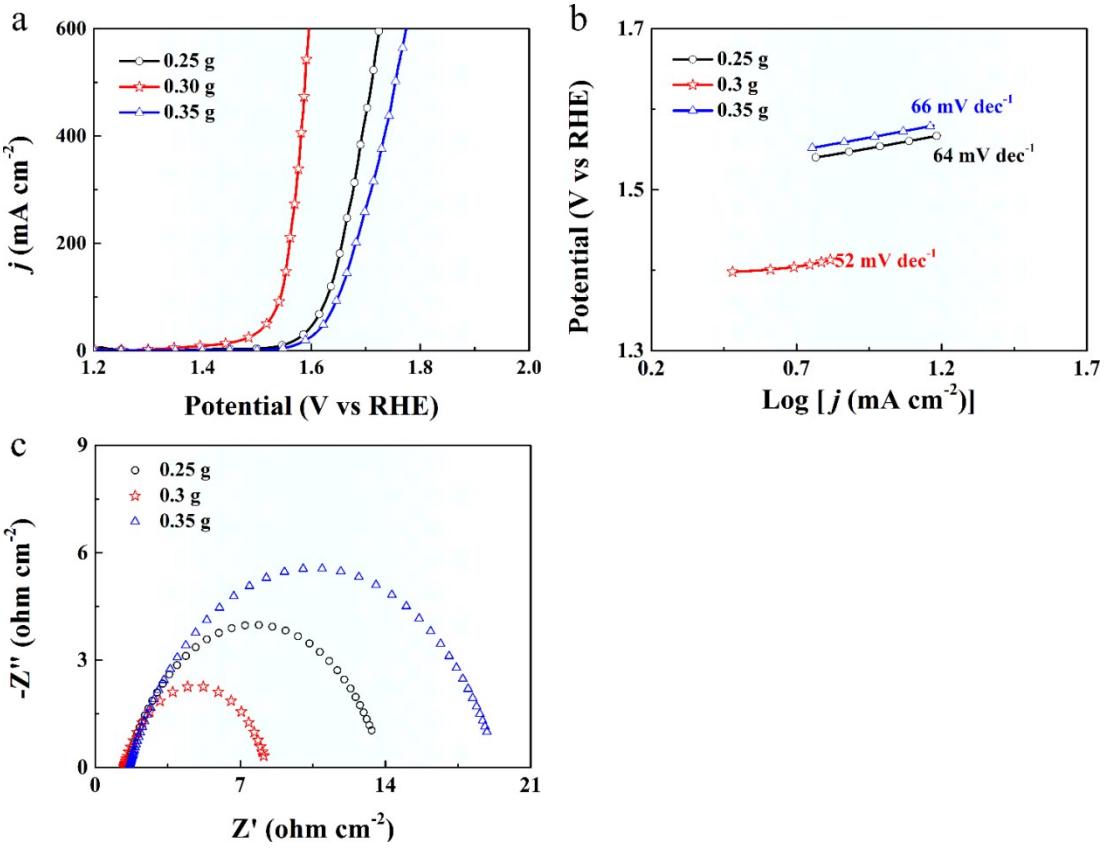

Figure S5. The effect of the red phosphorus mass on the OER activity of SnPi@CoP-Ni_5P_4/NCF in 1.0 M KOH electrolyte. (a) LSV curves and the corresponding Tafel slopes (b), and Nyquist curves (c).

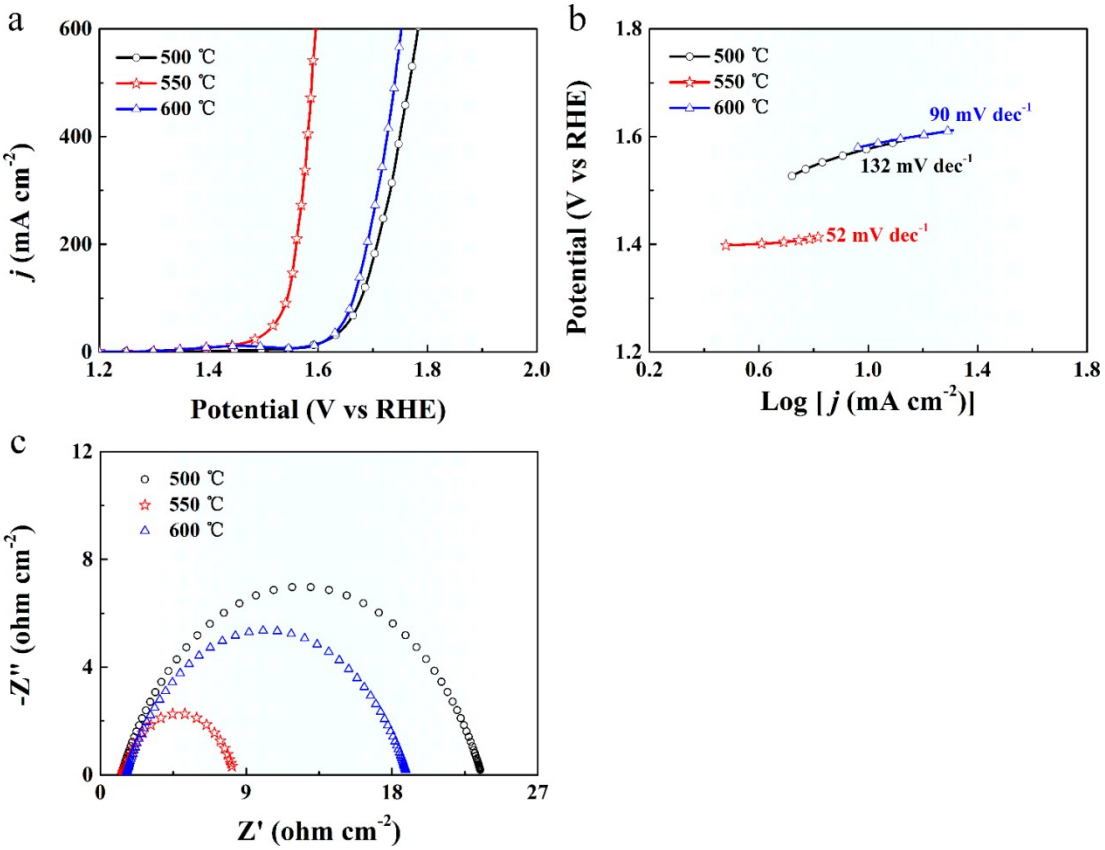

Figure S6. The influence of the phosphating reaction temperature on the OER activity of SnPi@CoP-Ni_5P_4/NCF sample in 1.0 M KOH. (a) LSV curves and the corresponding Tafel slopes (b), and Nyquist curves (c).

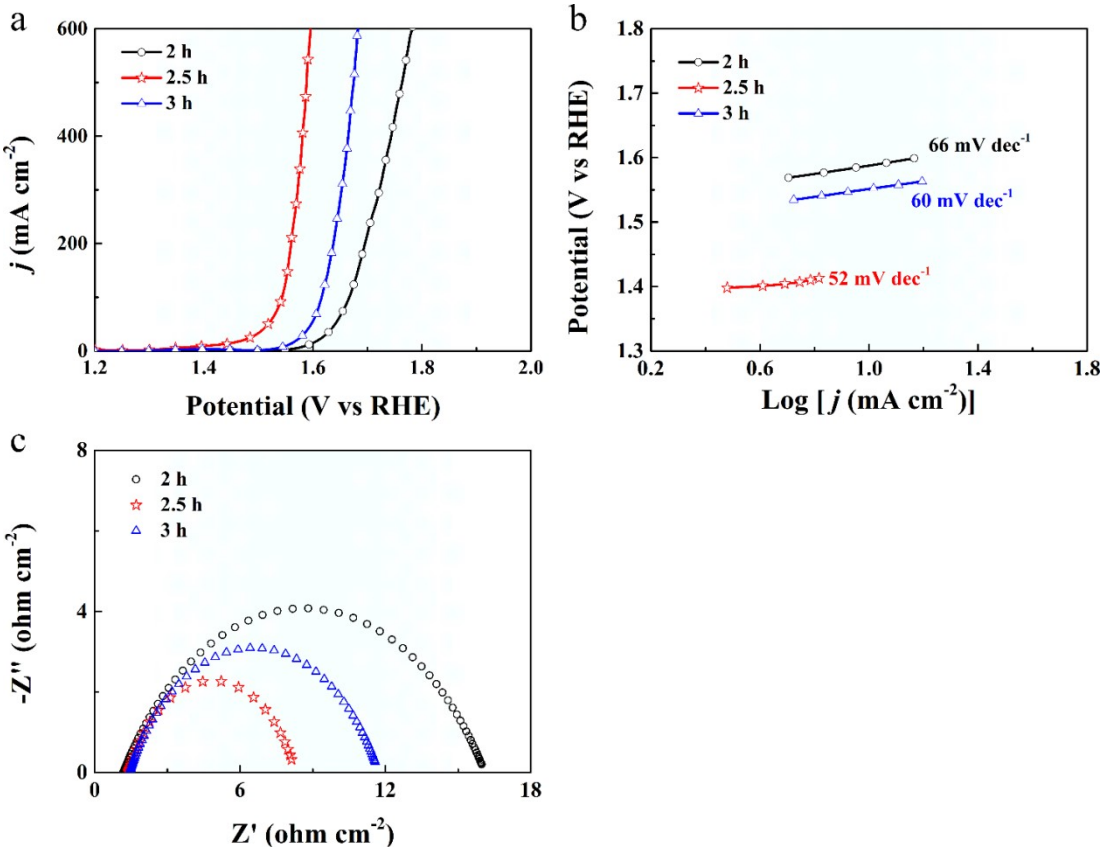

Figure S7. The influence of the phosphating reaction time on the OER activity of SnPi@CoP-Ni_5P_4/NCF sample in 1.0 M KOH. (a) LSV curves and the corresponding Tafel slopes (b), and Nyquist curves (c).

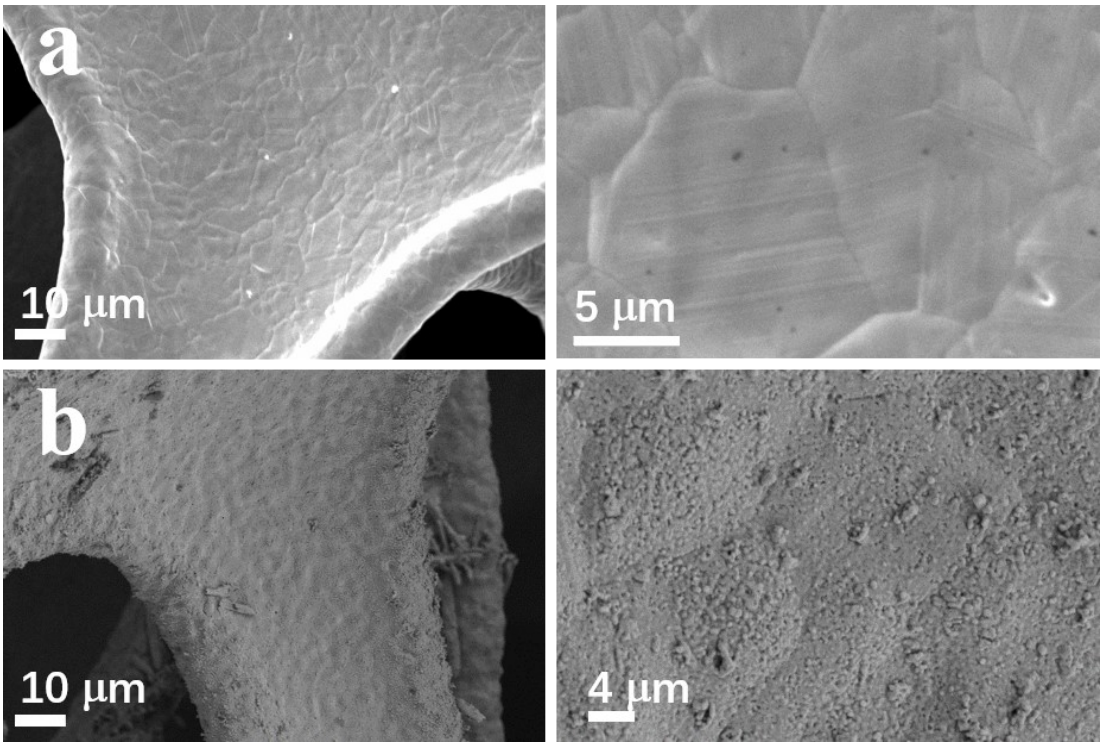

Figure S8. The SEM images of the fabricated Sn/NCF structure. (a) The original substrate, (b) Sn/NCF.

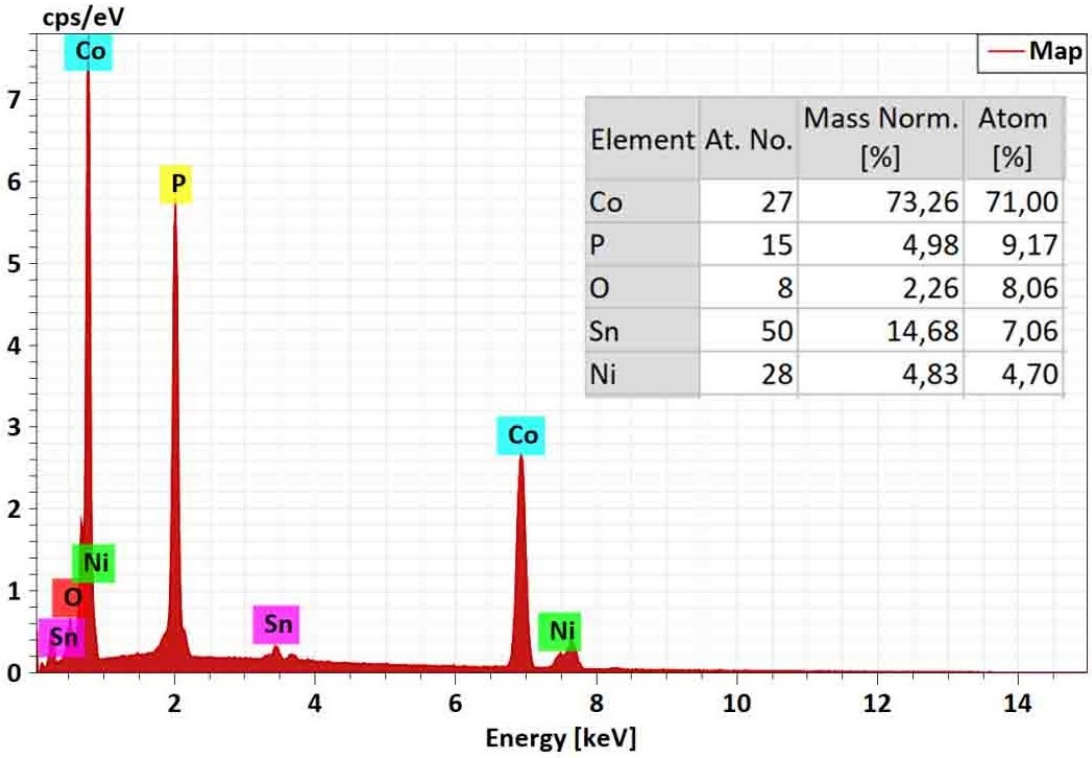

Element	At. No.	Mass Norm. [%]	Atom [%]
Co	27	73,26	71,00
P	15	4,98	9,17
O	8	2,26	8,06
Sn	50	14,68	7,06
Ni	28	4,83	4,70

Figure S9. The energy dispersive spectroscopy (EDS) of SnPi@CoP-Ni_5P_4.

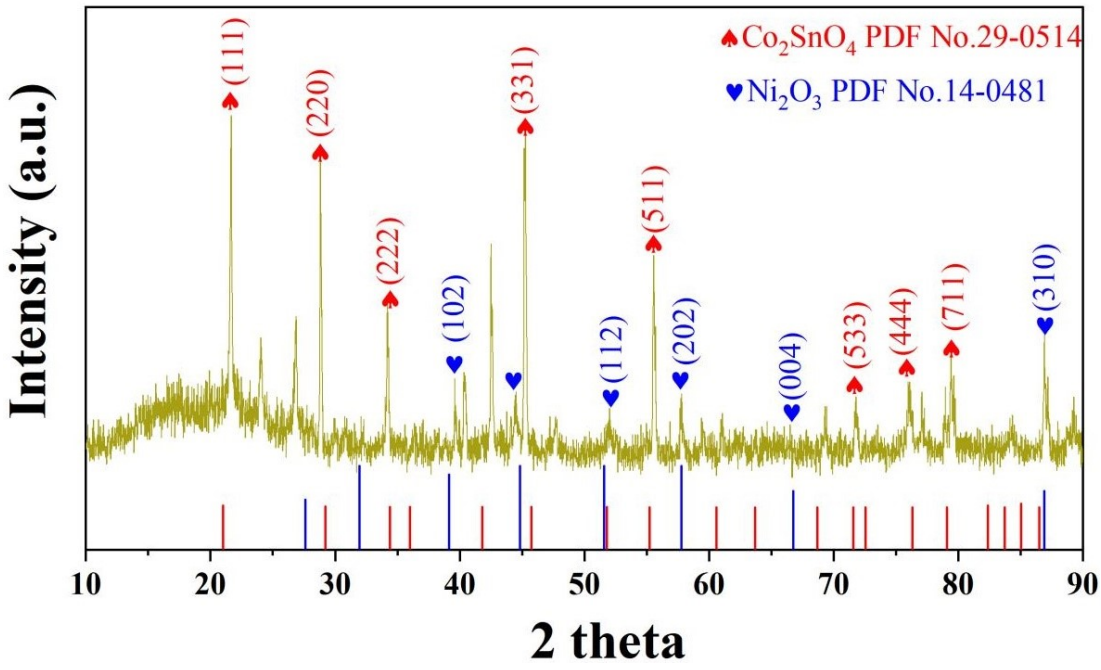

Figure S10. The XRD spectrum of the Ni_2O_3-Co_2SnO_4/NCF sample.

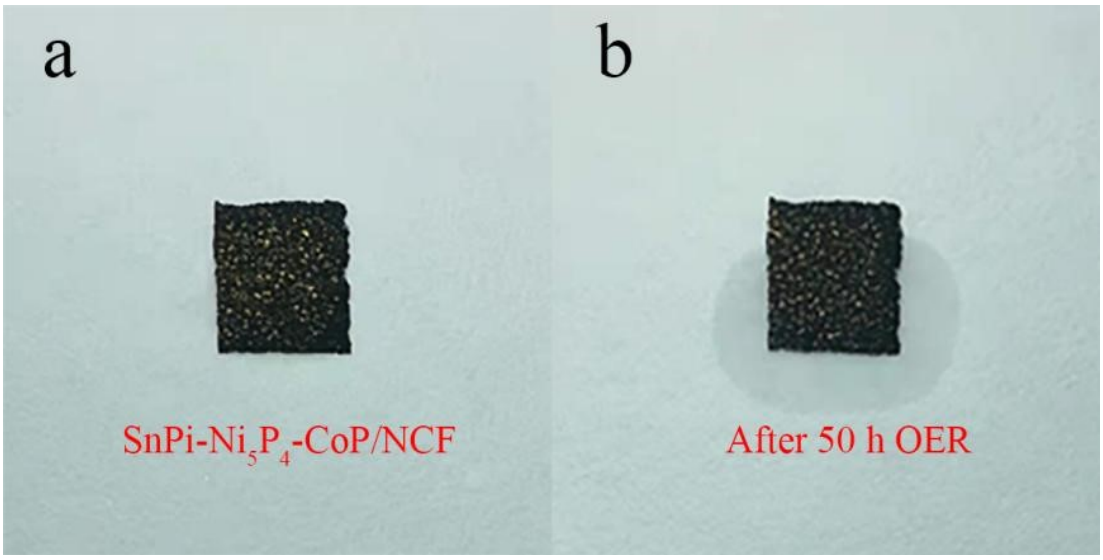

Figure S11. The macro-images of the SnPi@CoP-Ni_5P_4/NCF sample before (a) and after (b) 50 h OER tests at j_{10}.

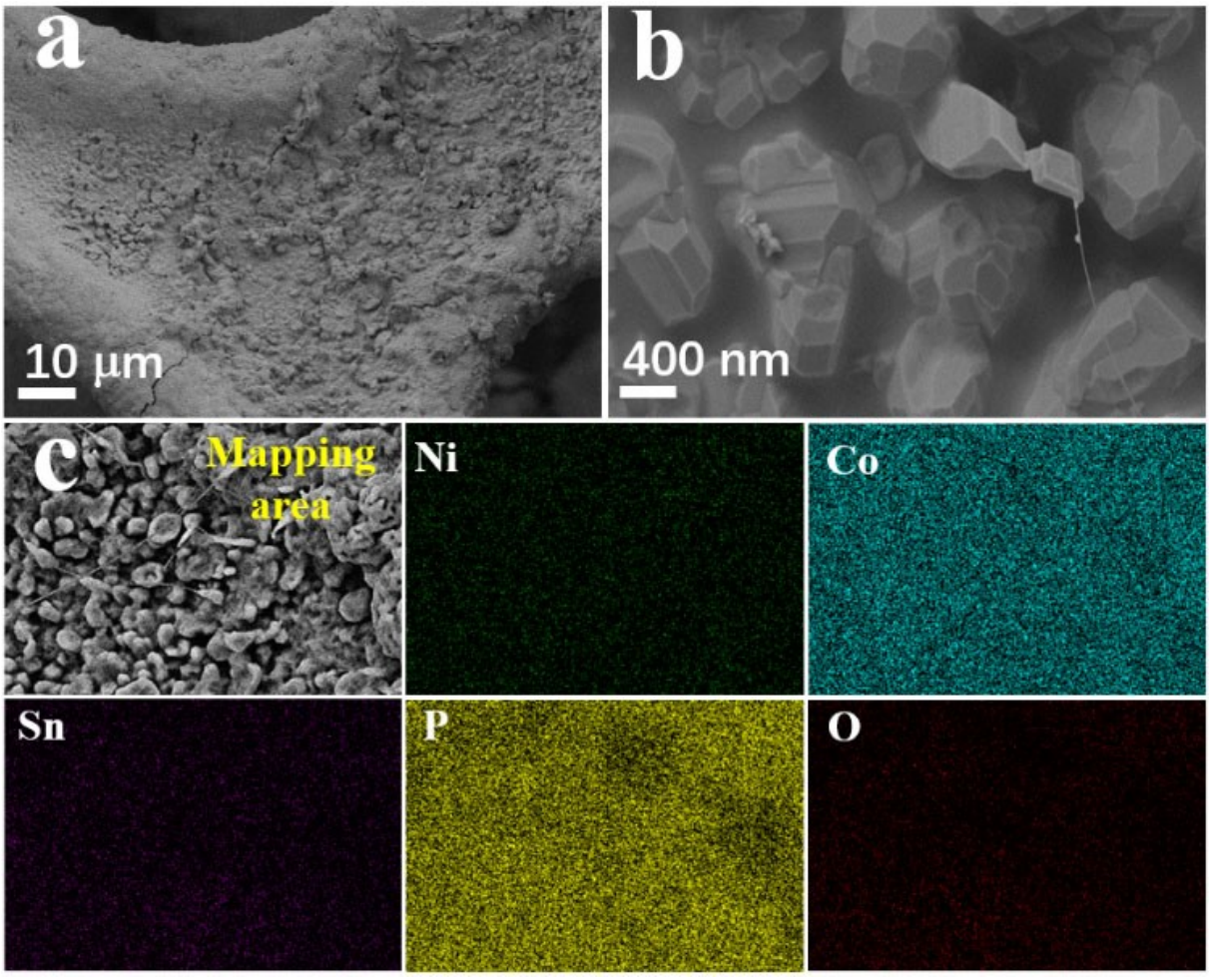

Figure S12. Physico-chemical structure characterization of the SnPi@CoP-Ni_5P_4/NCF sample after 50 h OER processes at a current density of j_{10}. (a) Low and (b) high resolution SEM images, (c) SEM mapping area of the sample and the corresponding distribution of Ni, Co, Sn, P and O elements, respectively.

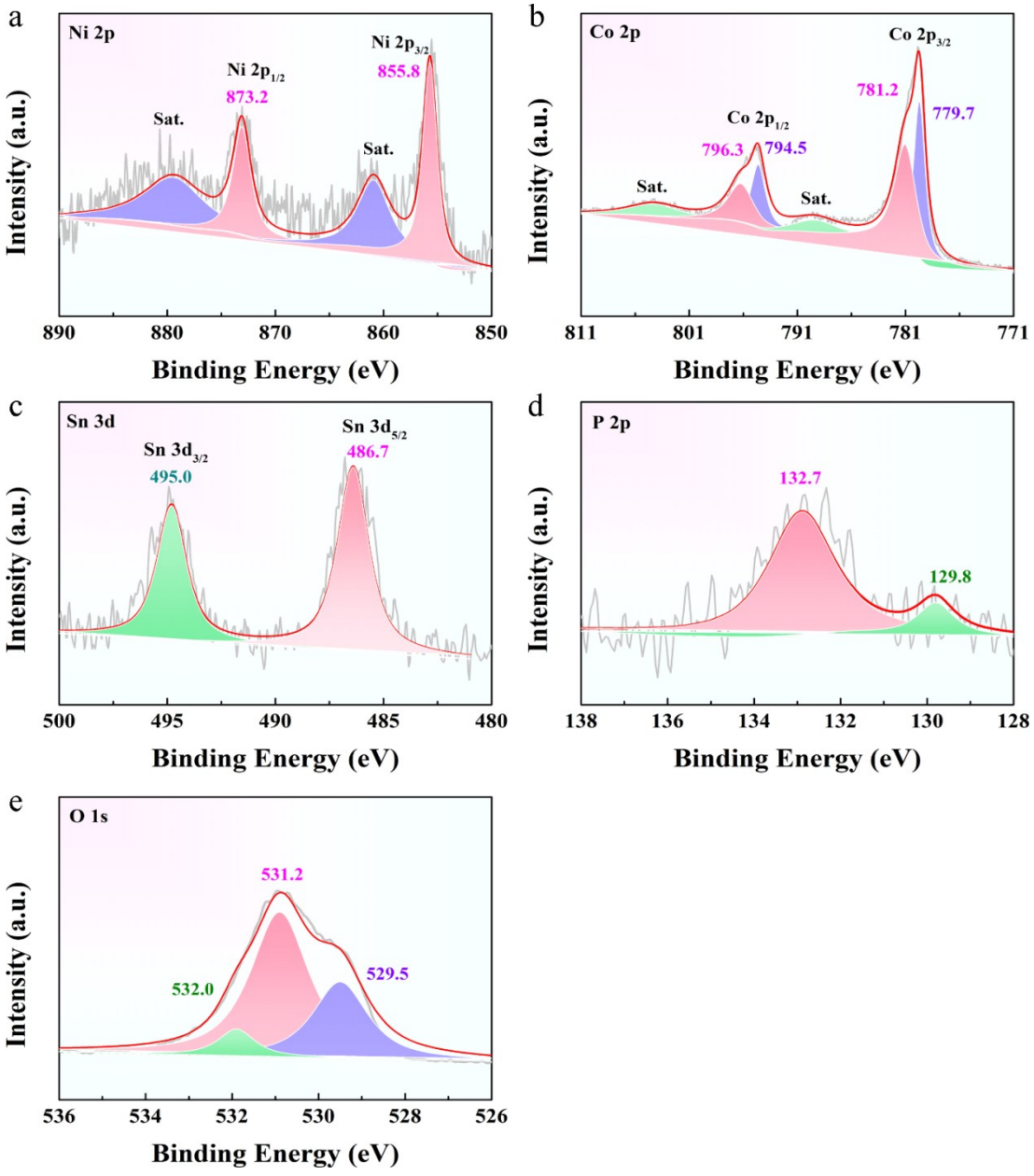

Figure S13. The XPS spectra of the SnPi@CoP-Ni_5P_4/NCF sample after 50 h OER process at the current density of 10 mA/cm^2.

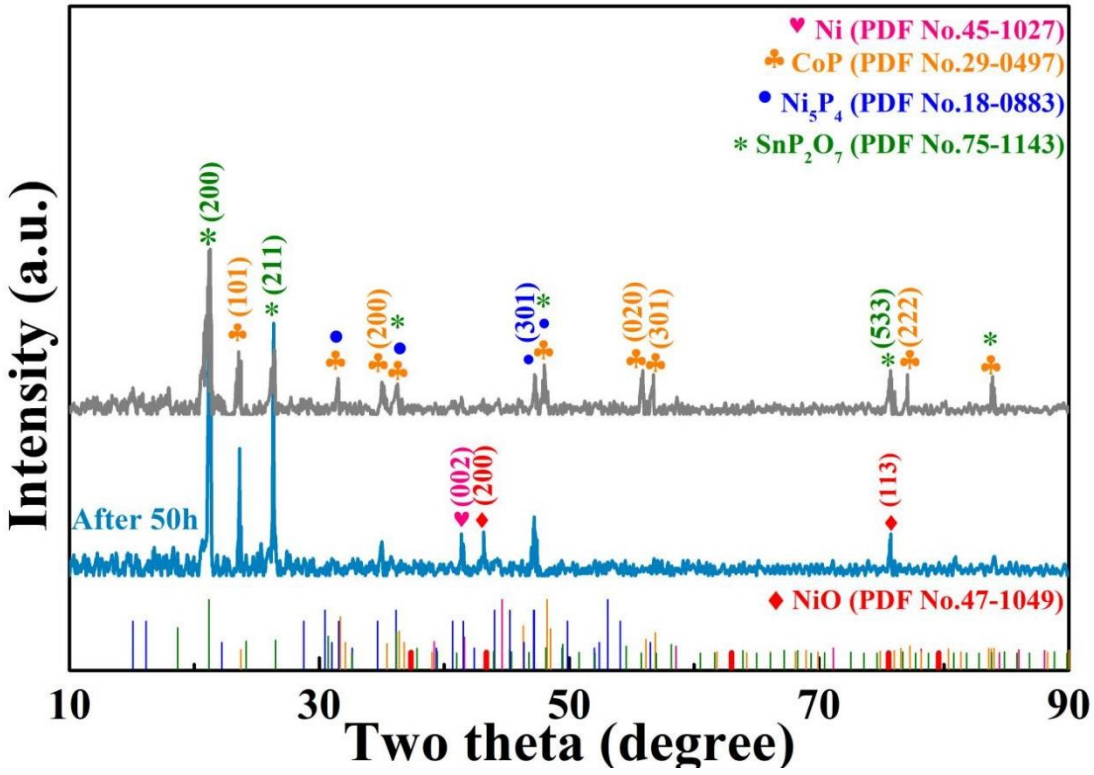

Figure S14. The XRD spectrum of the SnPi@CoP-Ni_5P_4/NCF sample after 50 h of the OER processes.

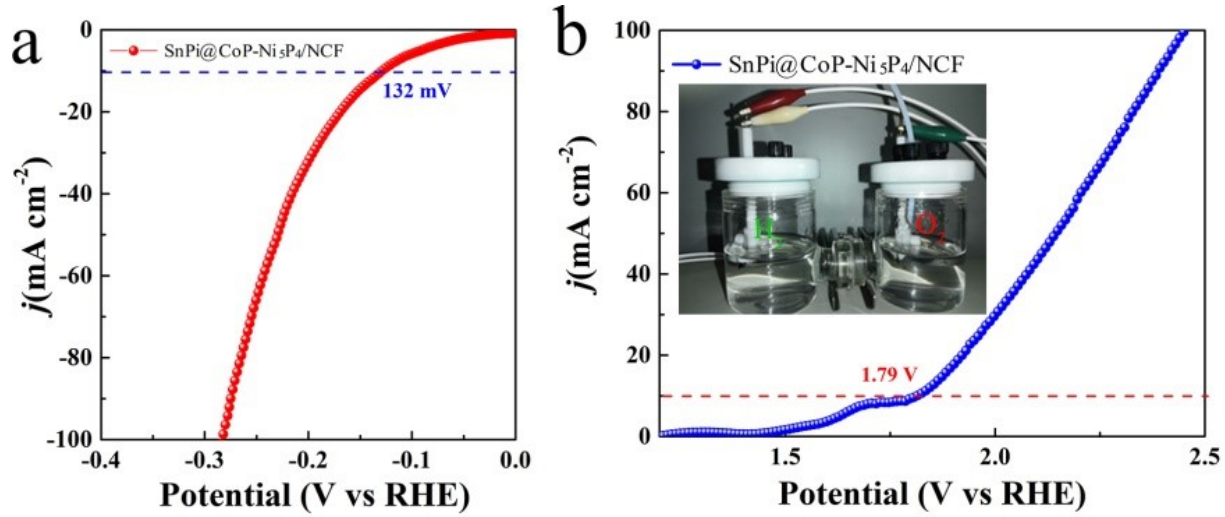

Figure S15. (a) Polarization curves of the SnPi@CoP-Ni_5P_4/NCF, (b) Performance of the bifunctional electrodes for overall water splitting; the inset is a photograph of the H-type cell.

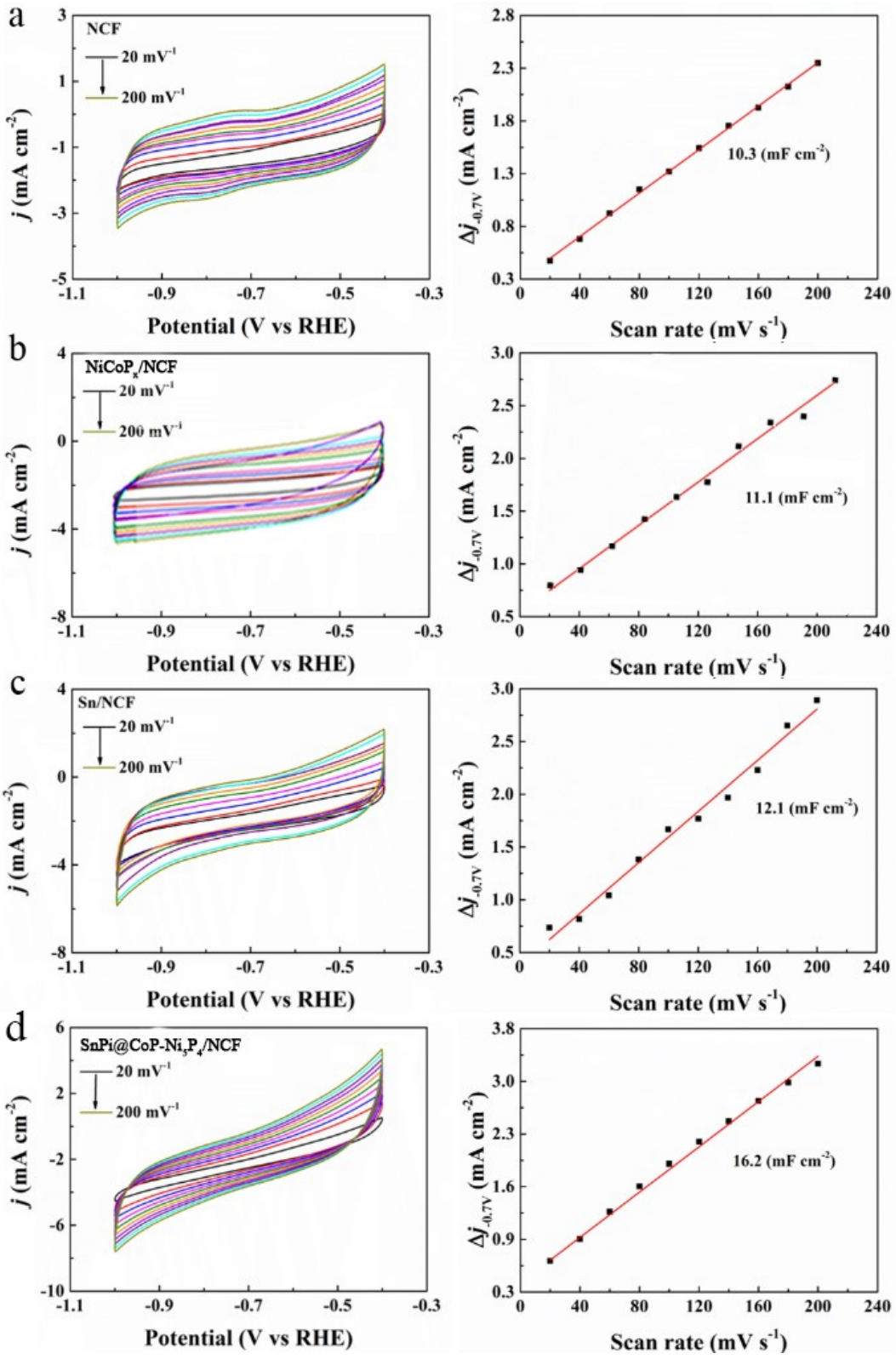

Figure S16. CV curves of the electrocatalysts with different scanning rate (left) and the corresponding C_{dl} (right). (a) NCF, (b) $NiCoP_x$/NCF, (c) Sn/NCF, and (d) SnPi@CoP-Ni_5P_4/NCF samples.

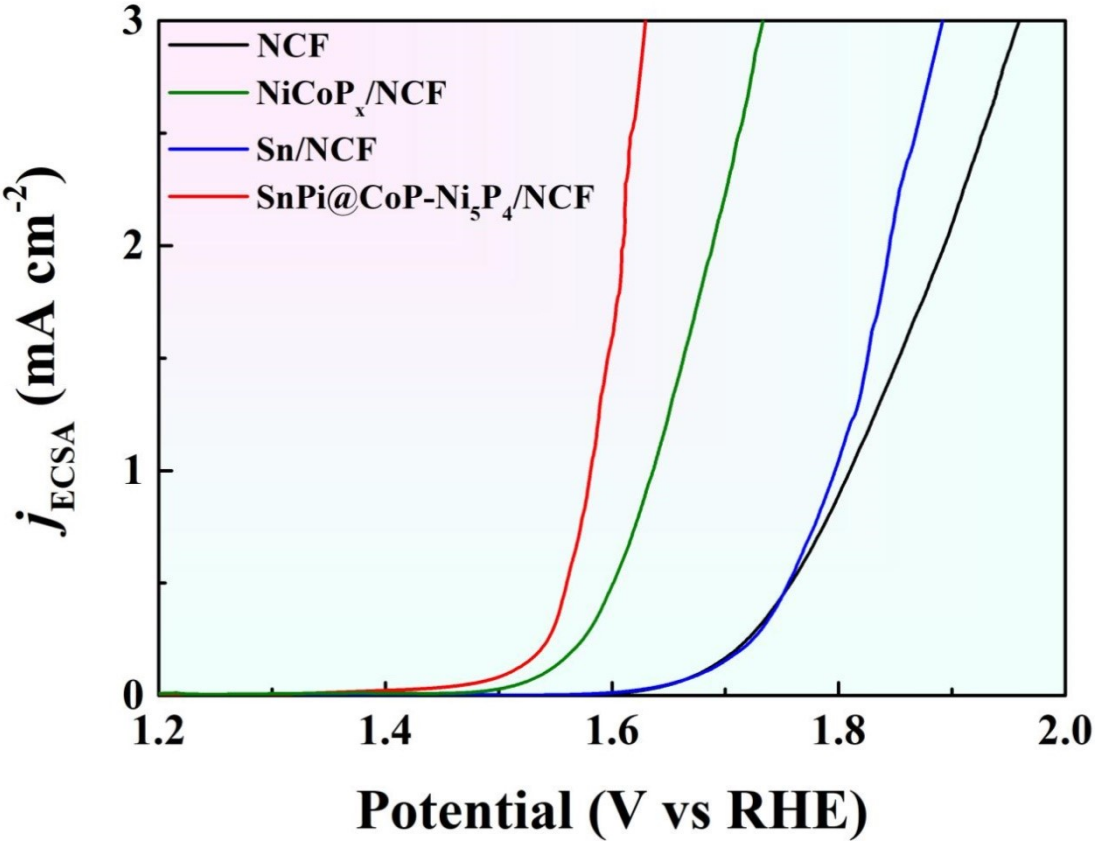

Figure S17. The LSV curves of the catalysts normalized with the electrochemical active surface area (ECSA = C_{dl}/Cs).

3. Supplementary Tables

Table S1. The elemental contents of different electrocatalysts.

Element / Atomic%	C 1s	O 1s	Ni 2p	Co 2p	Sn 4d	P 2p
SnPi@CoP-Ni_5P_4/NCF	23.43	46.15	2.46	10.34	3.59	14.03
After 50 h OER	15.32	58.81	2.58	20.83	0.26	2.21

Table S2. Comparison of electrocatalytic OER activity of various non-precious catalysts in 1.0 M KOH electrolyte.

Catalysts	η (mV) @ J (mA cm^{-2})	Tafel slope	Stability (h) @ J (mA cm^{-2})	References
SnPi@CoP-Ni_5P_4/NCF	180@10 309@100 364@600	52 mV dec^{-1}	50@10 50@100	This Work
$Co_{0.85}Se_{1-x}$@C	231@10 320@100	57 mV dec^{-1}	50@20	[S7]
Ir/Ni(OH)$_2$	224@10 270@100	41 mV dec^{-1}	6@20	[S8]
CoCuFeMoOOH@Cu	199@10 262@100	48.8 mV dec^{-1}	24@10 24@20 24@50	[S9]
Fe-Co_3O_4	262@10 303@100	43 mV dec^{-1}	50@10 50@100	[S10]
MoO_3/Ni-NiO	347@100	60 mV dec^{-1}	N/A	[S11]
$NiS_{0.5}Se_{0.5}$	257@10 310@100 320@200	61 mV dec^{-1}	300@10 300@100	[S12]
NiFc MOF/NF	195@10 241@100 262@200	44.1 mV dec^{-1}	40@10	[S13]
$NiCo_{2-x}Fe_xO_4$ NBs	274@10 330@100	42 mV dec^{-1}	25@10 25@50	[S14]
$NiFe(OH)_x$/(Ni,Fe)Se_2/CC	180@10	42 mV dec^{-1}	20@10	[S15]

	220@100 230@300			
Sn-Ni_5P_4	173@10 310@100	46 mV dec^{-1}	12@30 12@200 12@500	[S16]
LC-CoOOH NAs/CFC	294@10 345@100 370@200	70.73mV dec^{-1}	24@10	[S17]
Fe_xNi_yOOH-20F	280@100 348@500	66.7 mV dec^{-1}	160@200 70@500	[S18]
NiFe-Se/CFP	281@10 382@100	40.93 mV dec^{-1}	20@10	[S19]
a-NiHCF	210@50 280@400 309@800	53.45 mV dec^{-1}	30@160 30@242 30@260 30@287	[S20]

Table S3. TOF for RuO_2, SnPi@CoP-Ni_5P_4/NCF, and Sn/NCF catalysts at an overpotential of 160, 180, and 200 mV in the OER process.

TOF s^{-1}	**160 mV**	**180 V**	**200 mV**
RuO_2	5.9×10^{-4}	7.6×10^{-4}	8.2×10^{-4}
SnPi@CoP-Ni_5P_4/NCF	1.1×10^{-3}	1.3×10^{-3}	1.4×10^{-3}
Sn/NCF	2.1×10^{-4}	4.1×10^{-4}	1.6×10^{-4}

Table S4. The mass activity (MA) of OER active catalysts.

Sample	MA (mA g^{-1}@200 mV)
RuO_2	1.038×10^3
SnPi@CoP-Ni_5P_4/NCF	1.716×10^3
Sn/NCF	2.07×10^2

Table S5. Comparison of the amount of evolved O_2 on the electrodes containing various nonprecious metal catalysts.

Catalysts	Electrolytes	Current Density	H_2 generation amount	References
SnPi@CoP-Ni_5P_4/NCF	1.0 M KOH	10 mA cm^{-2}	1670 μmol h^{-1}	This Work
NiFe-LDHs	1.0 M KOH + 0.5 M NaCl	10 mA cm^{-2}	620 μmol h^{-1}	[S15]
$Ce_{0.2}$-IrO_2@NPC	0.5 M H_2SO_4	10 mA cm^{-2}	183 μmol h^{-1}	[S16]
Ni/LDH-ZnO	1.0 M KOH	10 mA cm^{-2}	290 μmol h^{-1}	[S23]
NiFe-Se/CFP	1.0 M KOH	10 mA cm^{-2}	87 μmol h^{-1}	[S19]
MoO_3/Ni-NiO	1.0 M KOH	10 mA cm^{-2}	176 μmol h^{-1}	[S11]
$NiS_{0.5}Se_{0.5}$	1.0 M KOH	10 mA cm^{-2}	187.5 μmol h^{-1}	[S12]
S-(Ni,Fe)OOH	1.0 M KOH + Seawater	500 mA cm^{-2}	1750 μmol h^{-1}	[S24]
δ-FeOOH/Ni_3S_2/NF	1.0 M KOH	10 mA cm^{-2}	90 μmol h^{-1}	[S25]
$Ni_{0.85}Fe_{0.15}PS$	1.0 M KOH	10 mA cm^{-2}	1674 μmol h^{-1}	[S26]
Fe@Fe_xNiO/Ni@Ni_yCoP	1.0 M KOH	25 mA cm^{-2}	111.6 μmol h^{-1}	[S27]
NiCoVP/NiFeVP	1.0 M KOH	10 mA cm^{-2}	35 μmol h^{-1}	[S28]
Gd-NiFe-LDH@CC	1.0 M KOH	10 mA cm^{-2}	196 μmol h^{-1}	[S29]
NiCoP-WO_x	1.0 M KOH	10 mA cm^{-2}	150 μmol h^{-1}	[S30]

References

S1 W. Kohn and L.J. Sham, *Phys. Rev.*, 1965, **140**, A1133.

S2 G. Kresse and J. Hafner, *J. Phys. Condens. Matter*, 1994, **6**, 8245.

S3 P.E. Blochl, *Phys. Rev. B*, 1994, **50**, 17953.

S4 J. Perdew, K. Burke and M. Ernzerhof, *Phys. Rev. Lett.*, 1996, **77**, 3865.

S5 S. Grimme, S. Ehrlich and L. Goerigk, *J. Comput. Chem.*, 2011, **32**, 1456–1465.

S6 B. Hammer and J. K. Nørskov, *Adv. Catal.*, 2000, **45**, 71-129.

S7 L. Zhang, C. J. Lu, F. Ye, R. L. J. Pang, Y. Liu, Z. Y. Wu, Z. P. Shao, Z. M. Sun and L. F. Hu, *Adv. Mater.*, 2021, **33**, 2007523.

S8 G. Q. Zhao, P. Li, N. Y. Cheng, S. X. Dou and W. P. Sun, *Adv. Mater.*, 2020, **32**, 2000872.

S9 L. J. Zhang, W. W. Cai and N. Z. Bao, *Adv. Mater.*, 2021, **33**, 2100745.

S10 S. L. Zhang, B. Y. Guan, X. F. Lu, S. B. Xi, Y. H. Du and X. W. Lou, *Adv. Mater.*, 2020, **32**, 2002235.

S11 X. P. Li, Y. Wang, J. J. Wang, Y. M. Da, J. F. Zhang, L. L. Li, C. Zhong, Y. D. Deng, X. P. Han and W. B. Hu, *Adv. Mater.*, 2020, **32**, 2003414.

S12 Y. Wang, X. P.Li, M. M. Zhang, Y. G. Zhou, D. W. Rao, C. Zhong, J. F. Zhang, X. P. Han, W. B. Hu, Y. C. Zhang, K. Zaghib, Y. S. Wang and Y. D. Deng, *Adv. Mater.*, 2020, **32**, 2000231.

S13 J. Liang, X. Gao, B. Guo, Y. Ding, P. Yan, P. Guo, P. Tse and J. Liu, *Adv. Mater.*, 2021, **133**, 12880–12884.

S14 Y. Huang, S. L. Zhang, X. F. Lu, Z. P. Wu, D. Y. Luan and X. W. Lou, *Angew. Chem. Int. Ed.*, 2021, **60**, 11841–11846.

S15 C. C. Liu, Y. Han, L. B. Yao, L. M. Liang, J. Y. He, Q. Y. Hao, J. Zhang, Y. Li and H. Liu, *Small*, 2021, **17**, 2007334.

S16 T. A. Shifa, K. Yusupov, G. Solomon, A. Gradone, R. Mazzaro, E. Cattaruzza and A. Vomiero, *ACS Catal.*, 2021, **11**, 4520–4529.

S17 S. H. Ye, J. P. Wang, J. Hu, Z. D. Chen, L. R. Zheng, Y. H. Fu, Y. Q. Lei, X. Z. Ren, C. X. He, Q. L. Zhang and J. H. Liu, *ACS Catal.*, 2021, **11**, 6104–6112.

S18 J. W. Xiao, A. M. Oliveira, L. Wang, Y. Zhao, T. Wang, J. H. Wang, B. P. Setzler and Y. S. Yan, *ACS Catal.*, 2021, **11**, 264–270.

S19 Y. J. Guo, C. R. Zhang, J. H. Zhang, K. Dastafkan, K. Wang, C. Zhao and Z. Q. Shi, *ACS Sustain. Chem. Eng.*, 2021, **9**, 2047–2056.

S20 X. Xu, T. Wang, L. Su, Y. Zhang, L. Dong and X. Miao, *Chem. Eng.*, 2021, **9**, 5693–5704.

S21 Q. Q. Tu, W. W. Liu, M. Jiang, W. J. Wang, Q. Kang, P. C. Wang, W. J Zhou and F. M. Zhou, *ACS Appl. Energy Mater.*, 2021, **4**, 4630–4637.

S22 Y. H. Wang, S. Y. Hao, X. N. Liu, Q. Q. Wang, Z. W. Su, L. C Lei and X. W. Zhang, *ACS Appl. Mater. Interfaces*, 2020, **12**, 37006–37012.

S23 Y. Luo, Y. H. Wu, D. H. Wu, C. Huang, D. Z. Xiao, H. Y. Chen, S. L. Zheng and P. K. Chu, *ACS Appl. Mater. Interfaces*, 2020, **12**, 42850–42858.

S24 L. Yu, L. B. Wu, B. McElhenny, S. W. Song, D. Luo, F. G. Zhang, Y. Yu, S. Chen and Z. F. Ren, *Energy Environ. Sci.*, 2020, **13**, 3439–3446.

S25 X. F. Ji, C. Q. Cheng, Z. H. Zang, L. L .Li, X. Li, Y. H. Cheng, X. J. Yang, X. F. Yu, Z. M. Lu, X. H. Zhang and H. Liu, *J. Mater. Chem. A*, 2020, **8**, 21199–21207.

S26 W. F. Peng, J. K. Li, K. Q. Shen, L. R. Zheng, H. Tang, Y. T. Gong, J. S. Zhou, N. Chen, S. J. Zhao, M. Y. Chen, F. M. Gao and H. Y. Gou, *J. Mater. Chem. A*, 2020, **8**, 23580–23589.

S27 Q. J. Che, X. Y. Zhou, Q. C. Liu, Y. Tan and Q. Li, *J. Mater. Chem. A*, 2021, **9**, 5833–5847.

S28 Y. Jeung, H. Jung, D. Kim, H. Roh, C. Lim, J. Han and K. Yong, *J. Mater. Chem. A*, 2021, **20**, 12203–12213

S29 M. Li, H. Li, X. C. Jiang, M. Q. Jiang, X. Zhan, G. T. Fu, J. M. Lee and Y. W. Tang, *J. Mater. Chem. A*, 2021, **9**, 2999–3006.

S30 D. Kim, Y. Jeong, H. Roh, C. Lim and K. Yong, *J. Mater. Chem. A*, 2021, **9**, 10909–10920.